Molecular mechanism of thioredoxin regulation in photosynthetic A_2B_2-glyceraldehyde-3-phosphate dehydrogenase

S. Fermani*, F. Sparla†, G. Falini*, P. L. Martelli‡, R. Casadio‡, P. Pupillo†, A. Ripamonti*, and P. Trost†§

*Department of Chemistry, University of Bologna, Via Selmi 2, 40126 Bologna, Italy; and †Laboratory of Molecular Plant Physiology and ‡Biocomputing Group, Department of Experimental Evolutionary Biology, University of Bologna, Via Irnerio 42, 40126 Bologna, Italy

Edited by Bob B. Buchanan, University of California, Berkeley, CA, and approved May 9, 2007 (received for review December 28, 2006)

Chloroplast glyceraldehyde-3-phosphate dehydrogenase (GAPDH) is a light-regulated, NAD(P)H-dependent enzyme involved in plant photosynthetic carbon reduction. Unlike lower photosynthetic organisms, which only contain A_4–GAPDH, the major GAPDH isoform of land plants is made up of A and B subunits, the latter containing a C-terminal extension (CTE) with fundamental regulatory functions. Light-activation of AB–GAPDH depends on the redox state of a pair of cysteines of the CTE, which can form a disulfide bond under control of thioredoxin *f*, leading to specific inhibition of the NADPH-dependent activity. The tridimensional structure of A_2B_2–GAPDH from spinach chloroplasts, crystallized in the oxidized state, shows that each disulfide-containing CTE is docked into a deep cleft between a pair of A and B subunits. The structure of the CTE was derived from crystallographic data and computational modeling and confirmed by site-specific mutagenesis. Structural analysis of oxidized A_2B_2–GAPDH and chimeric mutant $[A+CTE]_4$–GAPDH revealed that Arg-77, which is essential for coenzyme specificity and high NADPH-dependent activity, fails to interact with NADP in these kinetically inhibited GAPDH tetramers and is attracted instead by negative residues of oxidized CTE. Other subtle changes in catalytic domains and overall conformation of the tetramers were noticed in oxidized A_2B_2–GAPDH and $[A+CTE]_4$–GAPDH, compared with fully active A_4–GAPDH. The CTE is envisioned as a redox-sensitive regulatory domain that can force AB–GAPDH into a kinetically inhibited conformation under oxidizing conditions, which also occur during dark inactivation of the enzyme *in vivo*.

Calvin cycle | disulfide | light/dark | protein structure | redox

The ferredoxin/thioredoxin regulatory system represents a widespread mechanism of posttranslational modification of metabolic enzymes found in photosynthetic eukaryotes and cyanobacteria (1). The system involves ferredoxin, ferredoxin: thioredoxin reductase, a diversified family of plastid thioredoxins, and a large number of protein targets. Several enzymes of the Calvin cycle of CO_2 fixation are modulated in this way, allowing the flux of carbon assimilation to keep pace with the production of chemical energy by light reactions of photosynthesis (2, 3). No consensus sequences shared by thioredoxin-target proteins are known, and only in a few instances has the structural basis of regulation been elucidated in plants (4–6). In general, redox regulation depends on a couple of redox-active cysteines of the target protein, which undergo dithiol/disulfide equilibration with thioredoxins under physiological conditions. Chloroplast thioredoxins are reduced in the light and, in turn, impose a reduction state on target proteins, usually resulting in deinhibition of day-active enzymes (2, 3).

Chloroplast GAPDH catalyzes the single reductive step of the Calvin cycle of photosynthetic carbon assimilation. A finely regulated GAPDH isozyme specific of plants is constituted by two types of subunits (A and B) and is regulated by thioredoxin *f* (7). The fully active enzyme is heterotetrameric (A_2B_2) (8, 9). B subunits are 80% identical in sequence to A subunits, except they contain an additional extension of 30 aa at the C terminus of subunits B (C-terminal extension, CTE) (10), which includes a pair of redox-active cysteines (11). Photosynthetic GAPDH can use either NADPH or NADH as electron donors but NADPH is kinetically preferred (12, 13). The NADPH-dependent activity of A_2B_2–GAPDH is efficiently down-regulated as a consequence of the formation of a disulfide bond within the CTE (11), i.e., under oxidizing conditions such as those occuring in chloroplasts in the dark (3, 14). A_2B_2–GAPDH is also regulated by pyridine nucleotides (8) and the substrate 1,3-bisphosphoglycerate (15). Any type of regulation, however, ultimately depends on thioredoxin-sensitive CTE (10, 11, 16), including the NAD-induced aggregation of A_2B_2 into A_8B_8–GAPDH in darkness (8, 11, 17, 18).

The second NAD(P)H-dependent GAPDH isozyme of land plants, resembling enzyme forms of lower photosynthetic organisms (19), is a tetramer of A subunits without CTE (9, 20) and is correspondingly insensitive to regulation by thioredoxins and metabolites (11). However, it is reversibly inactivated by *S*-glutathionylation of catalytic Cys-149 (21). A chimeric mutant of A subunits fused with CTE, $[A+CTE]_4$–GAPDH, was recently found to be thioredoxin-regulated and prone to aggregate to oligomers, like native A_2B_2–GAPDH or recombinant B_4–GAPDH (22).

The CTE is evolutionarily derived from the regulatory peptide CP12 (23), an intrinsically unstructured protein (24). CP12 is involved in the regulation of GAPDH isoforms lacking regulatory B subunits, such as A_4–GAPDH of cyanobacteria (25, 26), *Chlamydomonas* (24) and higher plants (27, 28). B subunits are the result of a fusion between A subunits and the C-terminal half of CP12. As a result, AB–GAPDH of land plants gained an autonomous regulatory potential (29), but it still coexists with the CP12-dependent regulatory mechanism (30).

In this paper, we report on the tridimensional structures of oxidized A_2B_2–GAPDH and $[A+CTE]_4$–GAPDH, together with a functional characterization of site-specific mutants of B_4–GAPDH. The task of unraveling the sophisticated redox control mechanism of A_2B_2–GAPDH of land plants has been fulfilled by detailed structural and kinetic comparison of all these proteins with thioredoxin-independent A_4–GAPDH.

Author contributions: S.F. and F.S. contributed equally to this work; S.F., F.S., G.F., R.C., A.R., and P.T. designed research; S.F., F.S., G.F., and P.L.M. performed research; S.F., F.S., G.F., and P.T. analyzed data; and S.F., P.P., and P.T. wrote the paper.

The authors declare no conflict of interest.

This article is a PNAS Direct Submission.

Abbreviation: CTE, C-terminal extension of subunits B.

Data deposition: The atomic coordinates have been deposited in the Protein Data Bank, www.pdb.org [PDB ID codes 2PKQ (A_2B_2–GAPDH) and 2PKR ($[A+CTE]_4$–GAPDH)].

§To whom correspondence should be addressed. E-mail: trost@alma.unibo.it.

This article contains supporting information online at www.pnas.org/cgi/content/full/0611636104/DC1.

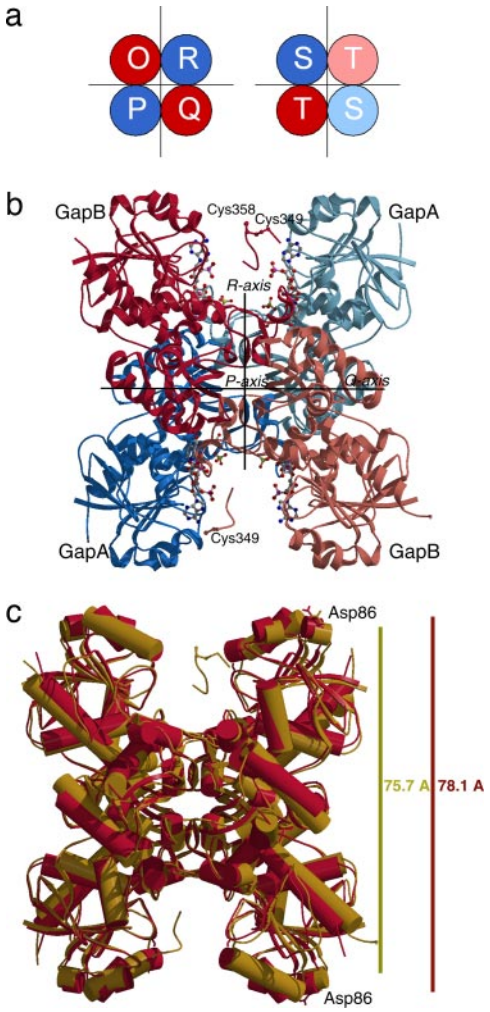

Fig. 1. Structural representation of oxidized A_2B_2–GAPDH complexed with NADP. (*a*) Schematic representation of the crystallographic model: a tetramer whose chains are named O, R, P, and Q, and a dimer ST, which generated a second tetramer by a crystallographic two-fold axis coincident with the molecular axis P. (*b*) Ribbon model of a single tetramer of oxidized A_2B_2–GAPDH. The coenzyme molecules, the sulfate ions of each subunit, and the cysteines of the CTE are represented as balls and sticks. (*c*) Superimposition of oxidized A_2B_2–GAPDH (gold) and recombinant A_4–GAPDH (red) tetramers (14), both complexed with NADP. The dimension of the tetramer along R-axis was measured between the C_α atoms of residues O86 and P86 or residues R86 and Q86. Helices are represented as cylinders and β-strands are represented as arrows. The images were produced by MOLSCRIPT (31) and rendered by Raster3D (32).

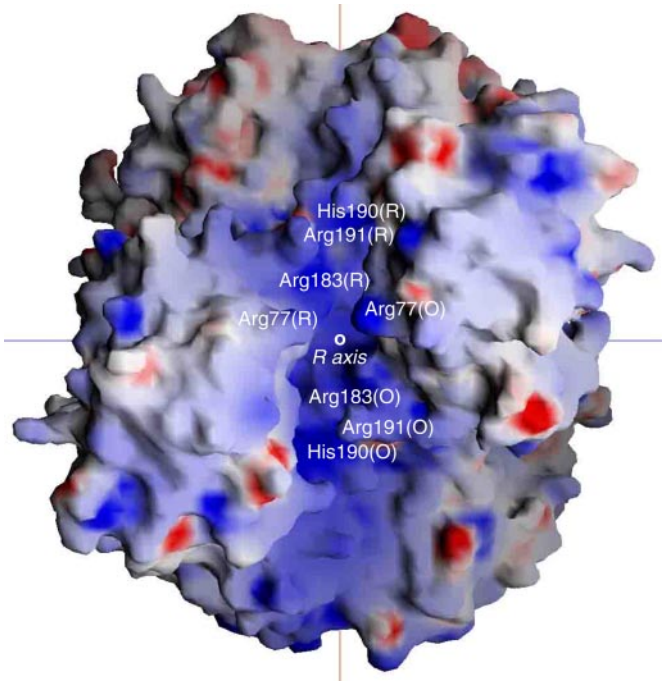

Fig. 2. Electrostatic surface potential of oxidized A_2B_2–GAPDH complexed with NADP. The sulfate ions present in the catalytic site of the crystallographic model are omitted from calculations. Blue depicts a positive potential and red depicts a negative one. The position of some residues is indicated. The tetramer is rotated by 90° along the Q axis with respect to Fig. 1 and viewed along the R axis. The relative potential scale ranges between -20 k_BT/e and $+20$ k_BT/e ($k_BT/e = 25.7$ mV at 298 K). The image was produced by GRASP (36).

Results

The crystallographic structural model of oxidized A_2B_2–GAPDH complexed with NADP is composed of one tetramer (indicated with chains O, P, Q, and R) and a dimer (chains S and T), which generates a second tetramer by using a crystallographic twofold axis coincident with the molecular axis P (Fig. 1 *a* and *b*). Chains O, Q, and T have been unequivocally identified as subunits B, whereas chains P, R, and S correspond to subunits A. Each type of subunits present in the asymmetric unit assumed a single backbone conformation. Superimposition of A to B subunits yields a rmsd of 0.570 Å on 333 C_α atoms.

The crystallographic structural model of oxidized $[A+CTE]_4$–GAPDH complexed with NADP is made up of three independent tetramers, each structurally reminiscent of A_2B_2–GAPDH. Both $[A+CTE]_4$ and A_2B_2–GAPDH showed an overall structural organization similar to thioredoxin-independent A_4–GAPDH (20). The three proteins were almost identical along axes P and Q but were differently sized along axis R, where the A_2B_2 and $[A+CTE]_4$ tetramers (75.7 and 77.2 Å, respectively) appeared to be shorter than A_4–GAPDH (78.1 Å) (Fig. 1*c*).

Similar to A_4–GAPDH subunits (20), all A_2B_2 and $[A+CTE]_4$ subunits consist of a coenzyme-binding domain and a catalytic domain [see supporting information (SI) Fig. 7]. This latter domain contains a long S-loop stretched out toward the R-axis-related subunit (from subunit A to B and vice versa; Fig. 1 and SI Fig. 7) (20), thus contributing to the coenzyme-binding site. One NADP molecule was bound to each coenzyme domain, and one or two sulfate ions deriving from the medium cocrystallized within each catalytic domain. These sulfate groups occupied two sites, named P_s and P_i, where the phosphate groups of the substrate 1,3-bisphosphoglycerate are allocated during catalysis (P_s for the C_3-phosphate and P_i for the C_1-phosphate) (33).

At variance from subunits A, native B subunits and recombinant A+CTE subunits (22) have an exclusive CTE from residue 335 to 362 (SI Fig. 7). This region was only partially detectable in our crystals. Inspection of $[2F_o - F_c]$ and $[F_o - F_c]$ electron-density maps showed an elongated electron-density region not continuous with any subunit and not fitted by the starting model but interpretable as a protein chain slipped into the wide, deep cleft bordered by a pair of A and B subunits (Fig. 1*b*). This density region was visible in both A_2B_2–GAPDH crystallographic tetramers OPQR and $(ST)_2$ but absent in $[A+CTE]_4$–GAPDH structure. Electrophoretic analysis of dissolved crystals showed that subunits B and subunits A+CTE tended to lose their CTE during crystal growth (15–20 days, data not shown) apparently because of proteolysis (a common occurrence in purified enzyme) (34, 35).

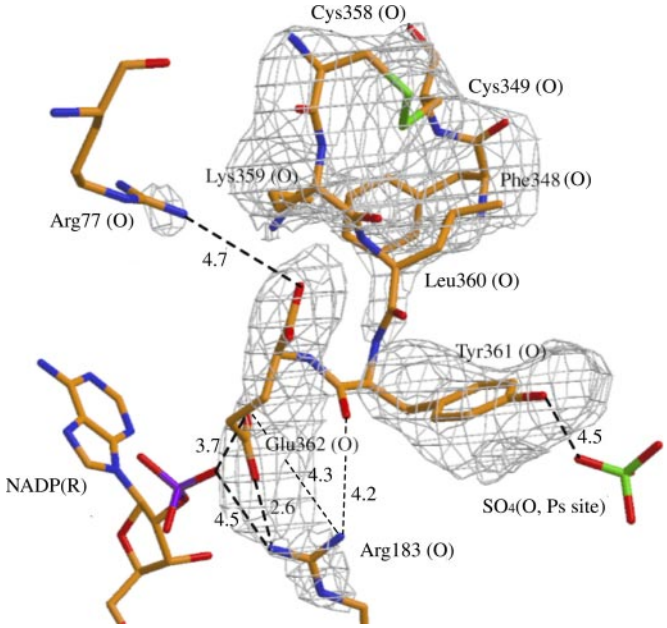

Fig. 3. [$F_o - F_c$] electron density of CTE (belonging to chain O) was calculated, omitting the CTE residues and shown at 2.5 σ cutoff. The disulphide bridge between Cys-349 and Cys-358 and distances below 5 Å between CTE residues and protein residues or ligands are also shown (see also SI Table 1). Atom color codes: carbon, yellow; oxygen, red; nitrogen, blue; sulfur, green; phosphorus, violet. The image was produced by Xtalview (37) and rendered by Raster3D (32).

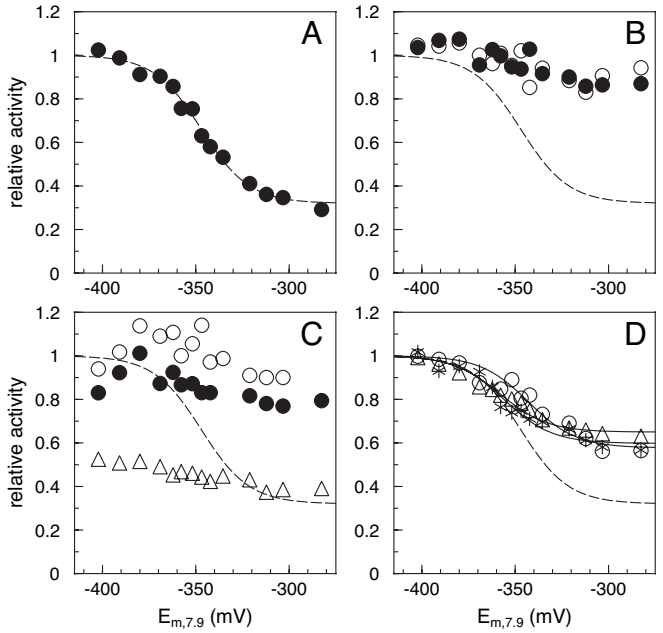

Fig. 4. Redox titration analysis (pH 7.9) of recombinant B_4–GAPDH and eight different site-specific mutants of B subunits. Each form displayed about the same NADPH-dependent specific activity under fully reducing conditions (set to 1), except mutant R77A, whose maximal specific activity was 50% in respect to the other forms (22). Data of mutants R77A and E362Q are taken from ref. 22. When significant, data points were fitted to the Nernst equation and the midpoint redox potential was calculated ($E_{m,7.9}$). (*A*) B_4–GAPDH ($E_{m,7.9} = -347$ mV). (*B*) Mutants E362Q (open circles) and R183A (filled circles). (*C*) Mutants R191A (filled circles), E356/357Q (open circles), and R77A (triangles). (*D*) Mutants E356Q (triangles, $E_{m,7.9} = -355$ mV), E357Q (asterisks, $E_{m,7.9} = -353$ mV), and D351N (open circles, $E_{m,7.9} = -345$ mV). In *B*, *C*, and *D*, the redox titration curve of B_4–GAPDH is shown as a broken line for comparison.

The cleft between A and B subunits featured a positive surface electrostatic potential because of the presence of six exposed arginines and two histidines (Arg-77, Arg-183, Arg-191, and His-190 conserved in both A and B subunits; Fig. 2). In the A_2B_2–GAPDH structure, the side chains of Arg-183 and Arg-191 exhibited an ordered conformation in all subunits (SI Table 1), pointing toward the electron-density region between A and B subunits. Arg-77 was also ordered in O, T, and S chains, but disordered in P, Q, and R chains. The exposed arginines of the cleft (Arg-77 and Arg-183, in particular; SI Table 1) had a well defined position in a majority of the subunits in the $[A+CTE]_4$–GAPDH structure also, recalling the A_2B_2 structure. In sharp contrast, recombinant spinach A_4–GAPDH complexed with NADP (13) showed disordered Arg-183 and Arg-191 whereas Arg-77 formed a salt bridge with the 2′-phosphate of NADP, which accounts for the marked kinetic preference of this active GAPDH for NADP (13).

The CTE contains several negatively charged residues (SI Fig. 7) and could be attracted by the strongly cationic cleft delimited by an A/B subunits pair. Indeed, the terminal tip of the CTE fitted the electron-density region not fitted by the starting model. In particular, the disulfide bridge between Cys-349 and Cys-358 had a clear electron density in chains O (Fig. 3 and SI Fig. 8) and T but was less defined in chain Q, and slightly different segments were inserted in different B subunits: Phe-348–Cys-349–SS–Cys-358-to-Glu-362 in chain O (Fig. 3 and SI Fig. 8), Cys-349–SS–Cys-358-to-Glu-362 in chain T, and Cys-358-to-Glu-362 in chain Q. In each B subunit, the tip of the CTE is devoid of secondary structure and can adopt different conformations with C-terminal Glu-362 facing Arg-183 and with both residues interacting also with NADP bound to A subunits (Fig. 3). Moreover, Tyr-361 interacted with the sulfate ion in the P_s site of the same B subunit (Fig. 3), and other interactions involving the CTE were observed in some but not all subunits (SI Table 2).

The role of the strong interaction between Glu-362 and Arg-183 in the docking of CTE as an autoinhibitory domain was tested by site-directed mutagenesis. The experiment was performed with recombinant regulatory B_4–GAPDH, known to be converted into a redox-insensitive form by mutation of Glu-362 into Gln (E362Q) (22). The mutation of Arg-183 into Ala (R183A) gives an identical result (Fig. 4). Both R183A and E362Q mutants are highly active with a definite kinetic preference for NADPH over NADH regardless of redox conditions. In this sense, they resemble A_4–GAPDH, which is always fully active because it does not contain a regulatory domain.

In both A_2B_2–GAPDH and $[A+CTE]_4$–GAPDH structures, NADP molecules are bound in extended conformation to each coenzyme domain and set in place by similar interactions with the respective subunits (Fig. 5). Because the 2′-phosphate group of the adenine ribose is the only chemical difference between NADP and NAD, interactions with this phosphate are relevant for the NADPH-dependent activity. In fact, the 2′-phosphate of NADP in A_4–GAPDH interacts with the side chain of Arg-77 of the same subunit and Ser-188 of the R-axis-related subunit (13), and comparable interactions occur in $[A+CTE]_4$. However, the behavior of oxidized A_2B_2–GAPDH was different. Whereas the 2′-phosphate of bound NADP in A subunits interacted with the R-axis-related B subunit through Arg-183 and Glu-362 (Fig. 3), the 2′-phosphate of NADP bound to B subunits failed to interact with any residue (Fig. 5). Lack of recognition of this 2′-phosphate group may contribute to the specific down-regulation of NADPH-dependent activity in oxidized A_2B_2–GAPDH (Fig. 4).

The structure of oxidized CTE was investigated by a computational approach predicting the positioning of whole CTE within our structural model based on crystallographic data. In the final model, which is very compatible with the crystalline

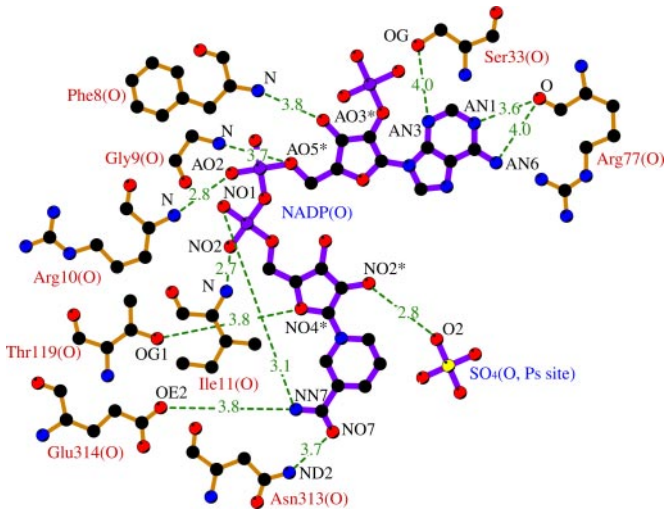

Fig. 5. Intermolecular and intramolecular hydrogen bonds of NADP bound to subunit B in oxidized A_2B_2–GAPDH. Distance values refer to chain O. The image was produced by LIGPLOT (38).

packing of oxidized A_2B_2–GAPDH, the CTE appeared in an extended conformation leaning against the protein surface. The CTE domain approached the coenzyme binding site with a loop stabilized by the regulatory disulfide between Cys-349 and Cys-358 (Fig. 6), and was kept in place through interaction of Arg-191 and Arg-77 with negative side-chains of the CTE, in addition to the salt bridge between Glu-362 and Arg-183. Consistently, mutation of Arg-191 into Ala (R191A) strongly diminished the redox sensitivity of B_4–GAPDH (Fig. 4), supporting the involvement of this residue in CTE docking. Mutation of Arg-77 into Ala (R77A; Fig. 4) was also recently shown to abolish redox sensitivity (22) and decrease NADPH-dependent activity, consistent with a crucial role of Arg-77 in kinetic efficiency of the enzyme. Although mutations of single negatively charged residues of the CTE potentially implicated in CTE docking (D351N, E356Q, and E357Q) only marginally affected the redox sensitivity of mutated proteins, complete redox insensitivity was achieved in the double mutant E356Q/E357Q (Fig. 4).

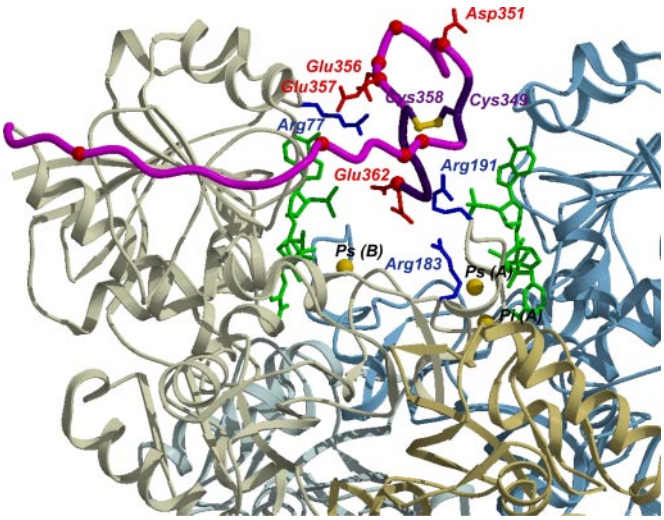

Fig. 6. Model structure of the CTE. Subunit B (chain O) and subunit A (chain R) are represented by beige and light cyan ribbons, respectively. The CTE is in cartoon representation; the segments that have been modeled with a computational procedure are magenta, and the residues placed on the basis of crystallographic data are purple. NADP coenzymes are green and the yellow spheres indicate the positions of the crystallized sulfate ions. The disulfide bond between Cys-349 and Cys-358 is highlighted in yellow. Residues whose relevance has been tested by site-directed mutagenesis are in ball and stick representation: negative residues of the CTE are red and positive residues of B subunit that are supposed to interact with the CTE are blue. The C_α atoms of all other negative residues of the CTE are represented by red spheres (from the N terminus of the CTE: Glu-336, Asp-343, Glu-346, Asp-347, Asp-355, see SI Fig. 7). The image was produced with MOLSCRIPT (31) and rendered with Raster3D (32).

The presence of oxidized CTE between each pair of A/B subunits not only affected the recognition of NADP but also the catalytic domains of the enzyme. Although the P_s site was fully occupied by a sulfate ion in each subunit of both A_2B_2 (Fig. 6 and SI Table 1) and $[A+CTE]_4$–GAPDH structures, this site was superimposable only in A and [A+CTE] subunits; it was displaced toward the S-loop and the CTE in B subunits (close enough to form an hydrogen bond with Tyr-361; Fig. 3). Different from the P_s site, the P_i site was partially vacant in A_2B_2–GAPDH structure. Where present (all A subunits and one B subunit), this second sulfate ion was located in the so-called "new P_i site" (39), i.e., closer than the "classical P_i site" to the catalytic essential residues Cys-149 and His-176 (33). The new P_i site in A subunits was associated with a particular conformation of the conserved region spanning from residue 205 to 214, resembling A_4–GAPDH complexed with NAD (40) (rmsd on 10 C_α atoms equal to 0.332 Å) more than B subunits with empty P_i sites (rmsd on 10 C_α atoms equal to 0.373 Å). In $[A+CTE]_4$–GAPDH structure, P_i sites were always occupied (SI Table 1), but in a few subunits, the sulfate ion was inserted between the new and classical P_i sites, and the conformation of segment 205–214 was varied from one subunit to the other. In all types of subunits (A, B, or A+CTE), however, the sulfate ion in the P_i site formed hydrogen bonds with Ser-148, Thr-150, Thr-208, and Gly-209. These subtle differences in the P-sites of the catalytic domains of A_2B_2, and $[A+CTE]_4$ may be related to the decreased kinetic efficiency of these enzymes in respect to fully active A_4–GAPDH.

Discussion

The regulation of A_2B_2–GAPDH in higher photosynthetic organisms represents a paradigmatic example of evolution of a thioredoxin-dependent regulatory mechanism in a photosynthetic enzyme. NAD(P)H-dependent GAPDH enzymes are involved in photosynthetic carbon assimilation in all oxygenic phototrophs. A_4–GAPDH isozymes are themselves thioredoxin-independent (11) but can be regulated through the action of free CP12, an intrinsically unstructured protein of chloroplasts (23, 24, 26, 28). A pair of C-terminal cysteines of CP12 can form an internal disulfide, and a second disulfide can form in the N-terminal moiety of the molecule in most species (19, 24, 25). In this oxidized conformation, the CP12 acts as a scaffold protein linking GAPDH to another important enzyme of the Calvin cycle, phosphoribulokinase (24–30), resulting in inhibition of both enzymes (28). This CP12-based mechanism of NAD(P)H–GAPDH regulation is widespread among oxygenic phototrophs (19, 23–30). However, whereas photosynthetic GAPDH is exclusively represented by homotetramers of A-type subunits in cyanobacteria and most eukaryotic algae, the major chloroplast GAPDH isozyme of land plants and some green algae contains both A and B subunits (19, 41), the latter consisting of A subunit fused at the C terminus with the C-terminal portion of CP12. This gene fusion gave rise to the redox-sensitive C-terminal extension of B subunits (CTE) (10, 23) and a further B subunit-dependent type of regulation of land plants, alongside with the CP-12 based one (29, 30). A and B subunits of chloroplast GAPDH form A_2B_2 heterotetramers displaying strong redox sensitivity (7, 11), which associate into inhibited hexadecamers (A_8B_8) under oxidizing conditions and low NADP(H)/NAD(H) ratios (8). The C-terminal extension of B subunits plays an

essential role in promoting AB–GAPDH aggregation to higher oligomers, reminiscent of the scaffolding role of CP12 (29). Conversely, A_2B_2 heterotetramers are stabilized by high NADP(H)/NAD(H) ratios and high 1,3-bisphosphoglycerate and are further activated by reduced thioredoxin *f* (7, 11, 15, 18). At variance from A_4–GAPDH, therefore, A_2B_2–GAPDH is finely regulated by metabolites and thioredoxin *f* under control of the CTE. The fact that only the NADPH-dependent activity of the enzyme is subject to regulation has been important for the elucidation of regulatory mechanisms (29, 40).

In fully activated A_2B_2–GAPDH, the pair of cysteines of the CTE are reduced and the CTE has no effect on enzyme activity; the kinetic parameters measured in reduced A_2B_2–GAPDH resemble those of A_4–GAPDH (12, 13, 40). In these active tetramers, the 2′-phosphate group of NADP is recognized through interactions with Arg-77 and Ser-188 (the serine belongs to the R-axis-related subunit of the protein) (13). These tetramers assume a distinctive conformation in the crystal, with P-sites fully occupied by sulfate ions deriving from the crystallization medium.

Formation of an internal disulfide bond within the CTE (Cys-349–Cys-358), promoted by oxidized thioredoxin *f* (11), affects this optimal tetrameric conformation and specifically inhibits the NADPH-dependent activity. The C-terminal residue of the CTE (Glu-362) forms a salt bridge with Arg-183 located in the bottom of the cleft delimited by a pair of A/B subunits (Fig. 3). The necessity of this salt bridge for CTE binding and enzyme regulation is highlighted by site-specific mutants R183A and E362Q (Fig. 4). Under the constraint of the disulfide, the C-terminal portion of the CTE adopts a bulky conformation such that several negative charges of the CTE get close to the positively charged residues aligned on the surface of the cleft (e.g., Arg-191 and Arg-77), thus contributing to the docking of CTE. At the same time, Arg-77 of B subunits is displaced away from the 2′-phosphate of NADP by interaction with repetitive anionic residues in the vicinity of the disulfide bond (Glu-356-Glu-357) and because no other residues (e.g., Ser-188) (13) can now interact with the 2′-phosphate, bound NADP is no longer recognized (Figs. 5 and 6). As a consequence, the overall conformation of the tetramer is changed (Fig. 1*c*) and the P-sites are variously occupied by sulfate ions (Fig. 6). The k_{cat} of the NADPH-dependent reaction is decreased to the level of NADH activity, which remains unchanged (13). These data agree with the idea that failure of NADP recognition is at the origin of NADPH–GAPDH inhibition in darkness.

More evidence supports this argument. Mutant R77A of B_4–GAPDH barely prefers NADPH over NADH (22) and is completely redox-insensitive (Fig. 4). The crystal structure of mutant S188A of A_4–GAPDH also shows no interactions with the 2′-phosphate of NADP, and the k_{cat} of the NADPH-dependent reaction is as low as in oxidized AB–GAPDH (13). Interestingly, the overall conformation of S188A tetramer is different from A_4–GAPDH (13) and more similar to oxidized AB–GAPDH and to a recently crystallized apo-A_4–GAPDH (42).

In conclusion, present data support the view that A_2B_2–GAPDH inhibition by oxidized thioredoxin depends on the docking of the disulfide-structured, negatively charged CTE into the positively charged cleft delimited by A/B subunits. In this location, the CTE appears to interfere with the recognition of bound NADP by the crucial residues Arg-77 and Ser-188, thus leaving the tetramer in a kinetically inhibited conformation, unable to efficiently use NADPH as the preferred coenzyme.

Materials and Methods

Purification and Characterization of Wild Type A_2B_2–GAPDH, Chimeric $[A+CTE]_4$–GAPDH, and Site-Specific Mutants of B_4–GAPDH. A_2B_2–GAPDH was purified from spinach chloroplasts as described (35). All recombinant enzymes were expressed, purified, and redox titrated according to ref. 22. Site-specific mutants of recombinant B_4–GAPDH were obtained as described in ref. 13 with the PCR primers reported in SI Table 3.

Purified A_2B_2–GAPDH and $[A+CTE]_4$–GAPDH were oxidized by addition of 20 mM oxidized DTT in the presence of thioredoxin from *Escherichia coli*. After a 16-h incubation at 4°C, thioredoxins were removed and the enzymes were desalted in 25 mM K-phosphate (pH 7.5), 20 mM NADP, 20 mM oxidized DTT and concentrated to 10 mg/ml. Oxidation typically led to ≈50% inhibition of the NADPH-dependent activity.

Crystallization and Data Collection. Crystals of oxidized A_2B_2 and $[A+CTE]_4$–GAPDH, both complexed with NADP, were grown by vapor diffusion technique, either hanging or sitting drop, at 277 K. Reservoir solutions consisted of 2.0–2.5 M (for A_2B_2) or 1.5–1.2 M ammonium sulfate (for $[A+CTE]_4$) and 0.1 M potassium phosphate pH 7.0–8.0. Crystals with identical shapes and sizes grew also with 5% vol/vol glycerol added to the previous reservoirs.

Three sets of diffraction data from different crystals of A_2B_2 and one set for $[A+CTE]_4$–GAPDH were collected at the European Synchrotron Radiation Facility (Grenoble, France) and Elettra Synchrotron Light Source (Trieste, Italy), with a maximum resolution of 3.1 and 2.4 Å, respectively (SI Table 4). Data were processed with DENZO/SCALEPACK (43).

Structure Solution and Refinement. Both structures were solved by molecular replacement with the program AMoRe (44) by using the coordinates of wild-type recombinant A_4–GAPDH as a probe (Protein Data Bank ID code 1RM4) (13). The refinement of both structures was carried out by using CNS (45) and graphical building was performed with the program O (46). A total of 5% of the data were randomly selected for R_{free} calculations.

The electron-density map calculated after a rigid body refinement on molecular replacement solutions of A_2B_2–GAPDH allowed the identification of the B subunits. Initial cycles of the A_2B_2–GAPDH structure refinement were performed to a maximum resolution of 4.0 Å, and strict noncrystallographic symmetry was applied with a σ cutoff of 2. Subsequently, data were extended to 3.6 Å by using all observed reflections (σ cutoff 0), and noncrystallographic symmetry restraints with different weights on main-chain and side-chain atoms were applied. At this stage, all sequence substitutions, coenzyme molecules, sulfate ions, and CTE atoms were inserted into the model accordingly with the electron-density maps. The position of these residues was confirmed by calculating omit maps. CTE residues, NADP molecules, and sulfate ions were excluded from noncrystallographic symmetry restraints during refinement.

The refinement of $[A+CTE]_4$–GAPDH was performed at a resolution of 2.4 Å, with no σ cutoff. Refinement and geometry statistics of final models are shown in SI Table 4.

Computational Modeling. The conformation of the CTE, from residue 332 to 362, was modeled on the basis of the spots of poor electronic density deriving from the diffraction map. Basically, the problem consisted of joining the end of helix 314–332, the last well determined portion of the protein, with the positions reconstructed for the last five residues (Cys-358–Glu-362). Some more electronic density was present near Cys-358 and was attributed to its disulfide-bonding partner, Cys-349. Other density signals could not be attributed to specific residues, but gave information about the direction adopted by the CTE. Describing these constraints as spatial restraints, the CTE was modeled by means of Modeller 6.2 (47). Different models were built, with different parameter sets for the restraints and their stereochemical quality was evaluated with ProCheck (48) and PROSA (49). The best model was retained for the analysis.

We thank Sandra Scagliarini for technical help in protein purification, Prof. Giuseppe Zanotti for useful discussion, and the European Synchrotron Radiation Facility (Grenoble, France) and Elettra Synchrotron Light Source (Trieste, Italy) for access to synchrotron facilities. This work was supported by Ministero dell'Università e della Ricerca Grants FIRB 2003 and PRIN 2005.

1. Buchanan BB (1992) *Photosynth Res* 33:147–162.
2. Schürmann P, Jacquot JP (2000) *Annu Rev Plant Physiol Plant Mol Biol* 51:371–400.
3. Buchanan BB, Balmer Y (2005) *Annu Rev Plant Biol* 56:187–220.
4. Carr P, Verger D, Ashton AR, Ollis D (1999) *Structure (London)* 7:461–475.
5. Johansson K, Ramaswamy S, Saarinen M, Lemaire-Chamley M, Issakidis-Bourguet E, Miginiac-Maslow M, Eklund H (1999) *Biochemistry* 38:4319–4326.
6. Chiadmi M, Navaza A, Miginiac-Maslow M, Jacquot JP, Cherfils J (1999) *EMBO J* 18:6809–6815.
7. Wolosiuk RA, Buchanan BB (1978) *Plant Physiol* 61:669–671.
8. Pupillo P, Giuliani Piccari G (1975) *Eur J Biochem* 51:475–482.
9. Cerff R (1979) *Eur J Biochem* 94:243–247.
10. Baalmann E, Scheibe R, Cerff R, Martin W (1996) *Plant Mol Biol* 32:505–513.
11. Sparla F, Pupillo P, Trost P (2002) *J Biol Chem* 277:44946–44952.
12. Cerff R (1978) *Phytochemistry* 17:2061–2067.
13. Sparla F, Fermani S, Falini G, Zaffagnini M, Ripamonti A, Sabatino P, Pupillo P, Trost P (2004) *J Mol Biol* 340:1025–1037.
14. Ziegler H, Ziegler I (1965) *Planta* 65:369–380.
15. Trost P, Scagliarini S, Valenti V, Pupillo P (1993) *Planta* 190:320–326.
16. Li AD, Anderson LE (1997) *Plant Physiol* 115:1201–1209.
17. Scagliarini S, Trost P, Pupillo P, Valenti V (1993) *Planta* 190:313–319.
18. Baalmann E, Backhausen JE, Rak C, Vetter S, Scheibe R (1995) *Arch Biochem Biophys* 324:201–208.
19. Petersen J, Teich R, Becker B, Cerff R, Brinkmann H (2006) *Mol Biol Evol* 23:1109–1118.
20. Fermani S, Ripamonti A, Sabatino P, Zanotti G, Scagliarini S, Sparla F, Trost P, Pupillo P (2001) *J Mol Biol* 314:527–542.
21. Zaffagnini M, Michelet L, Marchand C, Sparla F, Decottignies P, Le Maréchal P, Miginiac-Maslow M, Noctor G, Trost P, Lemaire SD (2007) *FEBS J* 274:212–226.
22. Sparla F, Zaffagnini M, Wedel N, Scheibe R, Pupillo P, Trost P (2005) *Plant Physiol* 138:2210–2219.
23. Pohlmeyer K, Paap BK, Soll J, Wedel N (1996) *Plant Mol Biol* 32:969–978.
24. Graciet E, Gans P, Wedel N, Lebreton S, Camadro JM, Gontero B (2003) *Biochemistry* 42:8163–8170.
25. Wedel N, Soll J (1998) *Proc Natl Acad Sci USA* 95:9699–9704.
26. Tamoi M, Myazaki T, Fukamizo T, Shigeoka S (2005) *Plant J* 42:504–513.
27. Wedel N, Soll J, Paap BK (1997) *Proc Natl Acad Sci USA* 94:10479–10484.
28. Marri L, Trost P, Pupillo P, Sparla F (2005) *Plant Physiol* 139:1433–1443.
29. Trost P, Fermani S, Marri L, Zaffagnini M, Falini G, Scagliarini S, Pupillo P, Sparla F (2006) *Photosynth Res* 89:1–13.
30. Scheibe R, Wedel N, Vetter S, Emmerlich V, Sauermann SM (2002) *Eur J Biochem* 269:5617–5624.
31. Kraulis PJ (1991) *J Appl Crystallogr* 24:946–950.
32. Merritt EA, Bacon DJ (1997) *Methods Enzymol* 277:505–524.
33. Didierjean C, Corbier C, Fatih, M, Favier F, Boschi-Muller S, Branlant G, Aubry A (2003) *J Biol Chem* 278:12968–12976.
34. Zapponi MC, Iadarola P, Stoppini M, Ferri G (1993) *Biol Chem Hoppe-Seyler* 374:395–402.
35. Scagliarini S, Trost P, Pupillo P (1998) *J Exp Bot* 49:1307–1315.
36. Nicholls A, Sharp KA, Honig B (1991) *Proteins Struct Funct Genet* 11:281–296.
37. McRee DE (1992) *J Mol Graphics* 10:44–47.
38. Wallace AC, Laskowski RA, Thornton JM (1995) *Protein Eng* 8:127–134.
39. Kim H, Feil IK, Verlinde CLMJ, Petra PH, Hol WGJ (1995) *Biochemistry* 34:14975–14986.
40. Falini G, Fermani S, Ripamonti A, Sabatino P, Sparla F, Pupillo P, Trost P (2003) *Biochemistry* 42:4631–4639.
41. Figge RM, Schubert M, Brinkmann H, Cerff R (1999) *Mol Biol Evol* 16:429–440.
42. Camara-Artigas A, Hirasawa M, Knaff DB, Wang M, Allen JP (2006) *Acta Crystallogr F* 62:1087–1092.
43. Otwinowsky Z, Minor W (1997) *Methods Enzymol* 276:307–326.
44. Navaza J (2001) *Acta Crystallogr D* 57:1367–1372.
45. Brünger AT, Adams PD, Clore GM, DeLano WL, Gros P, Grosse-Kunstleve RW, Jiang JS, Kuszewski J, Nilges N, Pannu N, *et al.* (1998) *Acta Crystallogr D* 54:905–921.
46. Jones TA, Zou JY, Cowan SW, Kjeldgaard M (1991) *Acta Crystallogr A* 47:110–119.
47. Sali A, Blundell TL (1993) *J Mol Biol* 234:779–815.
48. Laskowski RA, MacArthur MW, Moss DS, Thornton JM (1993) *J Appl Crystallogr* 26:283–291.
49. Sippl MJ (1993) *Proteins Struct Funct Genet* 17:355–362.